Inorganic Chemistry

Article

pubs.acs.org/IC

Crystal Packing Effects on the Magnetic Slow Relaxation of Tb(III)-Nitronyl Nitroxide Radical Cyclic Dinuclear Clusters

Fabrice Pointillart,*[,†,‡] Kevin Bernot,[†,§,∥] Giordano Poneti,[†,⊥] and Roberta Sessoli[†]

[†]University of Florence, "Ugo Schiff" Chemistry Department & INSTM Research Unit, Via Della Lastruccia 3-13, 50019 Sesto Fiorentino, Florence, Italy

[‡]Organométalliques: Matériaux et Catalyse, UMR 6226 CNRS-UR1 Institut des Sciences Chimiques de Rennes, Université de Rennes 1, 35042, Rennes Cedex, France

[§]Université Européenne de Bretagne, Rennes, France

[∥]INSA, SCR, UMR 6226, F-35708 Rennes, France

[⊥]Università degli Studi Guglielmo Marconi, Via Plinio 44, 0193 Rome, Italy

Supporting Information

ABSTRACT: Four lanthanide-based nitronyl nitroxide radical cyclic molecular clusters of formula $[Ln(hfac)_3(NITPhPO(OEt)_2)]_2$ (Ln^{III} = Gd (**1**), Tb (**2A** and **2B**), and Dy (**3**) and $NITPhPO(OEt)_2$ = 4′-[2-(1-oxyl-3-4,4,5,5-tetramethylimidazoline)phenyl]diethoxylphosphine oxide) have been synthesized. Their X-ray structures have been solved and highlight two different crystal packings. For the particular case of the Tb^{III} derivative, both of them can be obtained. In **2A**, the molecules are well-isolated, while **2B** shows short contacts between N−O radical groups. Static magnetic studies on the Gd^{III} derivative (**1**) demonstrate that lanthanides and radicals are ferromagnetically coupled (J = 3.46 ± 0.04 cm^{-1}). Dynamic magnetic studies show that both compounds **2A** and **2B** exhibit single molecule magnet behavior. A comparison of their magnetic behaviors highlights that the crystal packing has a crucial influence on the temperature range in which the SMM behavior is observed. In the case of the well-insulated Tb^{III}-based derivative (**2A**), the SMM behavior is observed at higher temperatures and lower frequencies than for the one that presents close-packing between the molecules (**2B**). Comparisons are then possible only under an applied external magnetic field (0.2 T) with Δ = 27.5(6) and 21.0(5) K and $\tau_0 = 2.64(25) \times 10^{-9}$ and $1.76(20) \times 10^{-9}$ s for **2A** and **2B**, respectively.

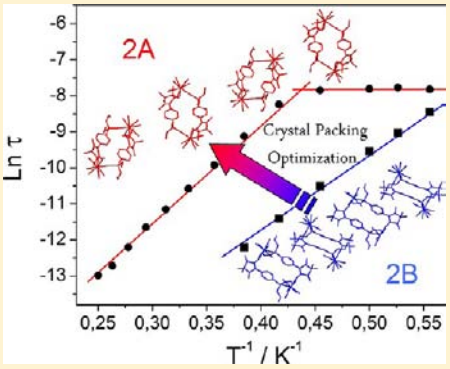

INTRODUCTION

Research on single-molecule magnets (SMMs) has been a very active field in the past two decades and has been rapidly expanding since the first magnetically bistable molecule, the mixed-valent dodecamanganese cluster (Mn12), was discovered in the early 1990s.[1] SMMs exhibit slow relaxation of the magnetization thanks to a large ground-state spin quantum number (S), a significant uniaxial magneto-anisotropy ($D < 0$), and a good magnetic isolation of the molecule.

Such phenomena can be enhanced if a ferromagnetic exchange interaction between anisotropic ions like Co^{II},[2] Mn^{III},[1,3] Tb^{III},[4] or Dy^{III} is present.[5] To do so, different bridging ligands have been used, and in particular organic radicals. They allow the building of complexes that present slow relaxation of the magnetization.[6] One of the most used organic radicals is without a doubt the stable nitronyl nitroxide radical, but only few of the published 2p−4f systems highlight a single molecule magnet or single chain magnet behavior.[7]

Nowadays, the challenge is to understand the effect of each of these parameters on the magnetic properties of SMMs. A promising strategy is to build families of isostructural compounds playing with the nature of the metal ion. The modification of the magnetic properties will then be directly attributed to the variation of the ion, every other parameter being unchanged. Such a strategy has allowed some of us to put in evidence the key role of the anisotropy of the metal ion in a lanthanide based single-chain magnet family.[7b] Another way is to use the ligands to tune some parameters of these molecular systems.[8] Coulon et al.[9] reported a family of single chain magnets incorporating different coordinated ligands on the axial positions and different counteranions. These structural changes affect then the magnetic properties. Very recently, some of us investigated the role of intramolecular ferromagnetic exchange interactions in trinuclear complexes $\{[Dy(hfac)_3]_2[M(bpca)_2]\}(CHCl_3)$ (M = Fe^{II}, Ni^{II}, $bpca^-$ = bis(2-pyridylcarbonyl)amine anion).[10] In these complexes, a diamagnetic substitution of part of the trinuclear units showed the importance of the noncollinearity of the Ising ions on the dynamic properties of a SMM. The same approach has been

Received: June 28, 2012
Published: November 5, 2012

   dx.doi.org/10.1021/ic301394x | *Inorg. Chem.* 2012, 51, 12218−12229

used to enlighten the effect of a weak intramolecular ferromagnetic coupling and β-diketonate ancillary ligands on the modulation of the dynamics of the magnetization in the complex $[Dy(hfac)_3(NITpPy)]_2$ (NITpPy = 2-(4-pyridy)-4,4,5,5-tetramethyl-4,5-dihydro-1*H*-imidazolyl-3-oxide)[7f] and $[Ln(Phtfac)_3(NITpPy)]_2$ (Ln^{III} = Gd, Tb, Dy and HPhtfac =4,4,4-trifluoro-1-phenylbutane-1,3-dione).[7h]

In this work, we have associated the nitronyl nitroxide substituted phosphine oxide $NITPhOP(OEt)_2$ to the Gd^{III} (**1**), Tb^{III} (**2A** and **2B**), and Dy^{III} (**3**) ions. The resulting compounds present an architecture that is similar to $[Dy(hfac)_3(NITpPy)]_2$, i.e. square molecules featuring the two lanthanides diagonally opposed. The Tb^{III} derivative crystallizes in two packing modes. One crystal packing leads to well isolated molecules (**2A**), whereas the other leads to short intermolecular contacts between the nitronyl nitroxide radicals of different molecular squares (**2B**).

The structure of the two Tb-based compounds has been determined by X-ray diffraction on single crystals. The nature of the intramolecular interaction between the lanthanide and the radical ligand has been understood thanks to the magnetic analysis of the isotropic Gd^{III} derivative (**1**). Finally, the confrontation of the magnetic properties of the two Tb^{III} derivatives (**2A** and **2B**) allows to highlight the effect of the intermolecular exchange interaction on the dynamics of the magnetization in lanthanide nitronyl-nitroxide based complexes.

EXPERIMENTAL SECTION

Synthesis. *General Procedures and Materials.* The whole synthesis of the 4′-[2-(1-oxyl-3-4,4,5,5-tetramethylimidazoline)-phenyl]diethoxylphosphine oxide ligand ($NITPhPO(OEt)_2$) was performed under an inert atmosphere. It was adapted from the synthesis of the 4′-[2-(1-oxyl-3-4,4,5,5-tetramethylimidazoline)-phenyl]diphenylphosphine oxide ligand.[11] The syntheses of **1**, **2A**, **2B**, and **3** were performed under aerobic conditions. The reagents were purchased from Aldrich and used as received without purifications. Starting lanthanides salts, $Ln(hfac)_3{\cdot}2H_2O$ (Ln^{III} = Gd, Tb, and Dy) were synthesized according to a literature method.[12]

(4-Bromophenyl)diethoxylphosphine ($P(OEt)_2PhBr$).[13] A solution of p-dibromobenzene (2.0 g, 8.5 mmol) in THF (6 mL) was added dropwise over a period of 1 h to a solution of *n*-BuLi (1.6 M in hexane, 5.3 mL, 8.5 mmol) kept at −70 °C. Afterward, diethyl chlorophosphite $PCl(OEt)_2$ (1.23 mL, d = 1.082 g mL^{-1}, 8.5 mmol) was slowly added and the reaction mixture stirred at room temperature for 8 h. After hydrolysis with H_2O (5 mL), the organic phase was extracted with Et_2O, washed with H_2O until the aqueous phase reached a pH = 7, and dried over $MgSO_4$. The solvent was removed in vacuo, leading to $P(OEt)_2PhBr$ as an oil which was used without further purification for the next step.

(4-Formylphenyl)diethoxylphosphine ($P(OEt)_2PhCHO$).[13a] A solution of $P(OEt)_2PhBr$ (1.0 g, 3.6 mmol) in THF (5 mL) was added dropwise over a period of 1 h to a solution of *n*-BuLi (1.6 M in hexane, 2.3 mL, 3.6 mmol) kept at −70 °C, followed by a solution of dimethylformamide DMF (0.3 mL, 3.9 mmol, in slightly excess) in THF (5 mL). The reaction mixture was then stirred for 7 h at room temperature. A total of 5 mL of H_2O was cautiously added and the mixture extracted with CH_2Cl_2. The organic layer was washed with H_2O, dried over $MgSO_4$, and evaporated to dryness to give $P(OEt)_2PhCHO$ as an oil, which was used without further purification for the next step.

4′-[2-(1,3-Dihydroxyl-4,4,5,5-tetramethylimidazoline)phenyl]-diethoxylphosphine. A solution of $P(OEt)_2PhCHO$ (1.0 g, 4.4 mmol) and 2,3-dimethyl-2,3-dihydroxyamino-butane (0.67 g, 4.4 mmol) in MeOH (20 mL) was refluxed for 12 h in a N_2 atmosphere. The resulting precipitate was filtered and washed with MeOH, yielding 4′-[2-(1,3-dihydroxyl-4,4,5,5-tetramethylimidazoline)phenyl]-diethoxylphosphine as a white solid. Yield: 0.97 g (62%). ^1H NMR ($CDCl_3$, 293 K, ppm): δ 7.50−7.20 (m, 4H, Ar); 4.51 (s, 1H, NCH); 2.49 (m, 4H, CH_2); 1.42 (t, 6H, Me); 1.11 and 1.06 (2s, 12H, Me).

4′-[2-(1-Oxyl-3-4,4,5,5-tetramethylimidazoline)phenyl]-diethoxylphosphine Oxide ($NITPhPO(OEt)_2$). A solution of $NaIO_4$ (0.44 g, 2.1 mmol) in H_2O (30 mL) was added to a suspension of 4′-[2-(1,3-dihydroxyl-4,4,5,5-tetramethylimidazoline)phenyl]-diethoxylphosphine (0.5 g, 1.4 mmol) in CH_2Cl_2 (60 mL). The reaction mixture was stirred for 15 min, and a deep blue color appeared in the organic phase, which was isolated, washed with H_2O, dried over $MgSO_4$, and evaporated to dryness. The residue was purified by chromatography over silica (eluent CH_2Cl_2/acetone 4:1). The mean blue band was collected and the solvent removed in vacuo. $NITPhPO(OEt)_2$ was obtained as a blue crystalline solid by slow evaporation of a CH_2Cl_2/hexane (1:1 in volume) solution. Yield: 274 mg (55%). Anal. Calcd (%) for $C_{17}H_{26}N_2O_5P_1$: C, 55.28; H, 7.05; N, 7.59. Found: C, 55.40; H, 7.19; N, 7.53.

*$[Gd(hfac)_3(NITPhPO(OEt)_2)]_2$ (**1**).* A total of 40.7 mg of $Gd(hfac)_3{\cdot}2H_2O$ (M = 814.3 g·mol^{-1}, n = 0.05 mmol) was dissolved in 15 mL of boiling *n*-heptane. The solution was kept at 45 °C, while 10 mL of a CH_2Cl_2 solution containing 18.5 mg of $NITPhPO(OEt)_2$ (M = 369 g·mol^{-1}, n = 0.05 mmol) was added. The mixture was stirred for 10 min and left without perturbation for slow evaporation. After one night, dark purple needles of **1**, suitable for X-ray diffraction, were obtained. Yield: 99.8 mg (87%). Anal. Calcd (%) for $C_{64}H_{58}N_4O_{22}F_{36}P_2Gd_2$: C, 33.45; H, 2.53; N, 2.44. Found: C, 33.41; H, 2.59; N, 2.39. IR (KBr): 1652, (s, C═O), 1608, 1525 (m), 1507 (m), 1361 (m, N−O), 1356 (m, N−O), 1256 (s, C−F), 1200, 1194 (s, P═O), 1145 (s), 796 (w), 664 (w), 548 (w) cm^{-1}.

*$[Tb(hfac)_3(NITPhPO(OEt)_2)]_2$ (**2A** and **2B**).* These two compounds have been synthesized with the same method described above. After one night, dark purple needles of **2A**·$2(CH_2Cl_2)$ (yield: 66.6 mg (58%)) and prisms of **2B** (yield: 28.7 mg (25%)) were obtained via slow evaporation. Both species of single crystals are suitable for X-ray diffraction. Anal. Calcd (%) for $C_{64}H_{58}N_4O_{22}F_{36}P_2Tb_2$: C, 33.41; H, 2.52; N, 2.44. Found: C, 33.34; H, 2.61; N, 2.51. IR (KBr): 1649 (s, C═O), 1609, 1529 (m), 1507 (m), 1360 (m, N−O), 1353 (m, N−O), 1255 (s, C−F), 1199, 1192 (s, P═O), 1147 (s), 797 (w), 664 (w), 543 (w) cm^{-1}.

*$[Dy(hfac)_3(NITPhPO(OEt)_2)]_2$ (**3**).* This compound has been synthesized with the same method described above. After one night, dark prisms of **3**, suitable for X-ray diffraction, were obtained via slow evaporation. Yield: 103.7 mg (90%). Anal. Calcd for $C_{64}H_{58}N_4O_{22}F_{36}P_2Dy_2$: C, 33.30; H, 2.51; N, 2.43. Found: C, 33.37; H, 2.50; N, 2.40. IR (KBr): 1650 (s, C═O), 1610, 1527 (m), 1507 (m), 1362 (m, N−O), 1356 (m, N−O), 1255 (s, C−F), 1201, 1194 (s, P═O), 1145 (s), 796 (w), 662 (w), 550 (w) cm^{-1}.

Physical Measurements. Single crystals of **1**−**3** were mounted on an APEXII Bruker-AXS diffractometer (Mo Kα radiation source, λ = 0.71073 Å, T = 150(2) K) for data collection, from the Centre de Diffractométrie (CDIFX), Université de Rennes 1, France. Structures were solved with a direct method using the SIR-97 program and refined with a full matrix least-squares method on F^2 using the SHELXL-97 program.[14] The X-ray structures reported in this paper present some disordered pending (ethoxy) and terminal (perfluorated) groups leading to some alerts in the checkcif files. In order to improve the quality of the crystal structures, some models of disorder have been used. Thus, for **1**, both ethoxy groups are disordered to two positions. The occupation factors are 0.67 and 0.33 as well as 0.50 and 0.50, respectively, for C14A−C15A and C14B−C14B, and C16A−C17A and C16B−C17B. The F7 and F9 fluorine atoms are also split with occupation factors of 0.61 and 0.39. For **2A**, the F31 and F33 fluorine atoms are also split with occupation factors of 0.58 and 0.42. For **2B** and **3**, the disorder comes from the two whole $hfac^-$ anions which are disordered on two positions with the global occupation factors of 0.59 and 0.41 as well as 0.59 and 0.41 for **2A** and **3**, respectively.

^1H NMR was recorded on a Bruker AC 300P spectrometer. Chemical shifts are reported in parts per million referenced to TMS for ^1H NMR.

dx.doi.org/10.1021/ic301394x | *Inorg. Chem.* 2012, 51, 12218−12229

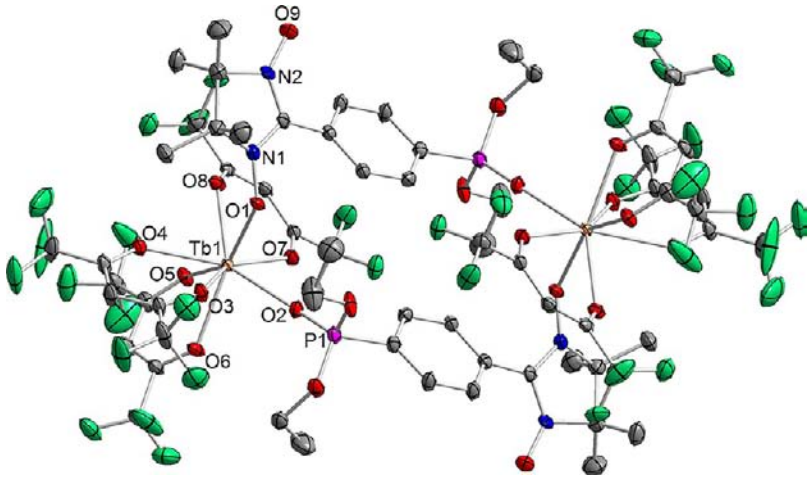

Figure 1. ORTEP view of the molecular structure of **2A** with thermal ellipsoids at 30% probability. Hydrogen atoms and solvent molecules are omitted for clarity.

Optical spectra were measured using a KBr disk method on a Perkin-Elmer 1600 Series Fourier transform infrared spectrometer (resolution 4 cm^{-1}) for IR.

All magnetic measurements were performed on pellets in order to avoid orientation of the very anisotropic materials. For **2A** and **2B**, the pellets were realized separating single crystals by hand. The dc-magnetic susceptibility measurements were performed with a Cryogenic S600 SQUID magnetometer between 2 and 300 K in an applied magnetic field of 0.05 T for temperatures in the range 2−250 K and 0.1 T for temperatures between 250 and 300 K. These measurements were all corrected for the diamagnetic contribution as calculated with Pascal's constants. The ac-magnetic susceptibility measurements were performed using a homemade ac probe operating in the range 100−25000 Hz.[15] For **2A** in zero-field, only an onset of SMM behavior is visible in the investigated T range. To limit overparametrization, the fitting procedures of $\chi''(\omega)$ plots of **2A** in zero field have been performed using the corresponding in-field parameters as input values. Then, a 10% evolution of the parameters is allowed step by step as the temperature is lowered.

RESULTS AND DISCUSSION

Synthesis. The three targeted lanthanides are Gd^{III}, Tb^{III}, and Dy^{III}. This choice has been made because the first ion is magnetically isotropic and allows easy estimation of the magnetic interaction (J), while the two others are the most efficient lanthanides to observe slow magnetic relaxation. All the compounds were obtained with a classic method which consists of increasing the Lewis acidity of the metallic center by the coordination of 1,1,1,5,5,5-hexafluoroacetyacetonate anions ($hfac^-$), followed by a dehydratation of the $Ln(hfac)_3{\cdot}2H_2O$ in a boiling *n*-heptane solution. The nitronyl nitroxide substituted phosphine oxide ligand $NITPhPO(OEt)_2$ is added to the resulting anhydrous $Ln(hfac)_3$, and after slow crystallization from a heptane/CH_2Cl_2 solution, single crystals of $[Ln(hfac)_3(NITPhPO(OEt)_2)]_2$ were obtained. In the case of Ln^{III} = Gd and Dy, only one form of single crystals was observed, while for Ln = Tb^{III}, two forms were observed: needles called **2A** (70%) and prisms called **2B** (30%). One has to note that the **2A** species appears before (after 12 h of slow evaporation) the **2B**. It has been impossible to find a synthetic strategy that affords directly pure derivatives. Consequently, the mother solution was filtered after 12 h to isolate the two species. Eventual byproducts can be easily removed by hand as the crystal shapes between **2A**·$2(CH_2Cl_2)$ (needles) and **2B** (prisms) are very different.

X-Ray Structure Descriptions. *$[Tb(hfac)_3(NITPhPO(OEt)_2)]_2{\cdot}2(CH_2Cl_2)$ (**2A**)·$2(CH_2Cl_2)$.* A view of the molecular structure of **2A**·$2(CH_2Cl_2)$ is shown in Figure 1. Selected bond lengths and angles are reported in Table 2. The asymmetric unit of **2A**·$2(CH_2Cl_2)$ is made of a $Tb(hfac)_3$ moiety, a $NITPhPO(OEt)_2$ ligand, and a dichloromethane molecule of crystallization. These two are bound through the oxygen atoms of the P═O groups. However, the organic radical binds another $Tb(hfac)_3$ moiety through one of its two N−O groups. The inversion center and this double bonding of the $NITPhPO(OEt)_2$ lead to the formation of the cyclic dimer $[Tb(hfac)_3(NITPhPO(OEt)_2)]_2$ **2A** as shown in Figure 1. **2A** is then a molecular rectangle featuring the long edge formed by the radical−metal bond through the P═O group and the shorter one by the same radical bound to the other ion through the N−O group. The distance between the Tb^{III} centers along the diagonal of the rectangle is 9.442(2) Å. Each TbIII ion is surrounded by eight oxygen atoms coming from three $hfac^-$ ligands, one phosphine oxide group, and one N−O group. The Tb−O range distance is 2.296(5)−2.417(6) Å. The oxygen O2 atoms of the P═O and N−O groups are coordinated in a cis orientation on the Tb^{III} ion (the O1−Tb1−O2 angle is 81.4(7)°). The coordination polyhedron of the Tb^{III} can be described as a slightly distorted dodecahedron. The mean distortion comes from the shorter $Tb1{-}O2_{(P=O)}$ distance (2.296(5) Å). All the other Tb−O distances are similar (2.387(6) Å). One can notice that the shorter $M{-}O_{(P=O)}$ bonds have been previously observed in the $[Mn(hfac)_2(p\text{-}PhPONIT)]_2$ molecular rectangle (where *p*-PhPONIT = 4′-[2-(1-oxyl-3-4,4,5,5-tetramethylimidazoline)phenyl]-diphenylphosphine oxide ligand).[16] These bond length differences influence the shape of the coordination polyhedron of the lanthanide ion. In fact a regular bicapped square face trigonal prism is characterized by the following four angles: $\alpha1 = 0°$, $\alpha2 = 21.8°$, and $\alpha3 = \alpha4 = 48.2°$.[17] The $\alpha1$, $\alpha2$, $\alpha3$, and $\alpha4$ angles are described by the angle between the planes (O2O6O7; O5O6O7), (O1O4O8; O1O3O4), (O4O5O6; O4O5O8), and (O1O2O7; O1O2O3), respectively. In **2A**, the values of these angles have been found to be equal to 20.5(3)°, 28.4(3)°, 55.8(2)°, and 57.6(2)°. In other terms, the square face of the regular bicapped square face trigonal prism is folded by an angle of 21.3° (Figure 2). As a comparison, the tilting between the phenyl and the imidazole planes is greater in **2A** (38.6(3)°)

dx.doi.org/10.1021/ic301394x | *Inorg. Chem.* 2012, 51, 12218−12229

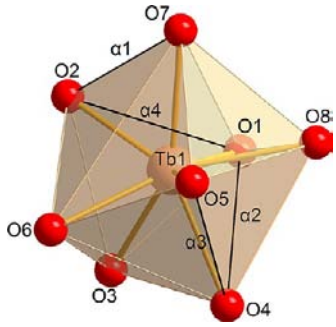

Figure 2. Tb^{III} polyhedron in **2A** with characteristic angles.

than it is in $[Mn(hfac)_2(p\text{-PhPONIT})]_2$ (27°),[16] in the N-coordinated NITpPy compounds $[Dy(hfac)_3(NITpPy)]_2$ (33.5°)[9] and in $[Mn(hfac)_2(NITpym)]_2$ (32°) (NITpym = 2-(5-pyrimidinyl)-4,4,5,5-tetramethyl-4,5-dihydro-1H-imidazoline-1-oxyl-3-oxide).[18] This difference is due to the different nature of the metal ion in the first case and to a diverse radical in the last one. In the $[Mn(hfac)_2(NITm\text{-Py})]_2$ (NIT*m*-Py = 2-(3-pyridyl)-4,4,5,5-tetramethyl-4,5-dihydro-1H-imidazoline-1-oxyl-3-oxide), the tilting angle is close to the one found in our complex (38.7° and 43.7°,[18] respectively).

When analyzing a crystal packing involving nitronyl–nitroxide derivatives, one has to closely look to the NO groups. In fact, because of the strongly delocalized electron densities along their O–N–C–N–O system, nitronyl–nitroxide ligands are able to transmit intermolecular magnetic interaction even when the distances between the complex seem to be very large.[7g] In **2A**, the shortest distance between N–O groups is an intramolecular contact equal to 8.835(10) Å, while the shortest intermolecular contact is equal to 8.953(11) Å. Hence, there are no significant intermolecular contacts between the magnetic rectangles. The shortest intermolecular Tb–Tb distance is 9.240(9) Å, and each cyclic dimer is well isolated from the others due to the perfluorated moieties that are localized in the periphery of the molecule (Figure 3).

*$[Tb(hfac)_3(NITPhPO(OEt)_2)]_2$ (**2B**).* A view of the molecular structure of **2B** is shown in Figure 4. Though **2B** is very similar to **2A** from a molecular point of view, significant differences in the coordination sphere symmetry have been identified. The characteristic angles take now the following values 16.2(3)°, 18.2(2)°, 37.2(2)°, 37.9(2)° and 16.3(2)°, 16.6(2)°, 37.5(2)°, 39.5(2)° for Tb1 and Tb2 respectively. The two Tb^{III} environments can be considered similar in **2B** but they are quite different that the one observed in **2A**. The crystal packing is totally different. In **2B**, short intermolecular contacts between the O–N–C–N-O systems takes place (Figure 5) with distances of about 4 Å that can be compared with the distance of 10.246(25) Å observed in **2A** (Figure 6). The shortest intra- and intermolecular Tb–Tb distances are similar than **2A** with 9.487(28) Å and 10.317(30) Å respectively.

*$[Gd(hfac)_3(NITPhPO(OEt)_2)]_2$ (**1**) and $[Dy(hfac)_3(NITPhPO(OEt)_2)]_2$ (**3**).* The X-ray structure of **1** (Tables 1 and 2, Figure S1) shows that this compound is very similar to **2A**. The slight changes of the crystallographic parameters are due to the dichloromethane molecules of crystallization in **2A** which are not in **1**. In any cases, **1** and **2A** can be considered magnetically isolated. Compound **3** (Tables 1 and 2, Figure S2) is isostructural to **2B**.

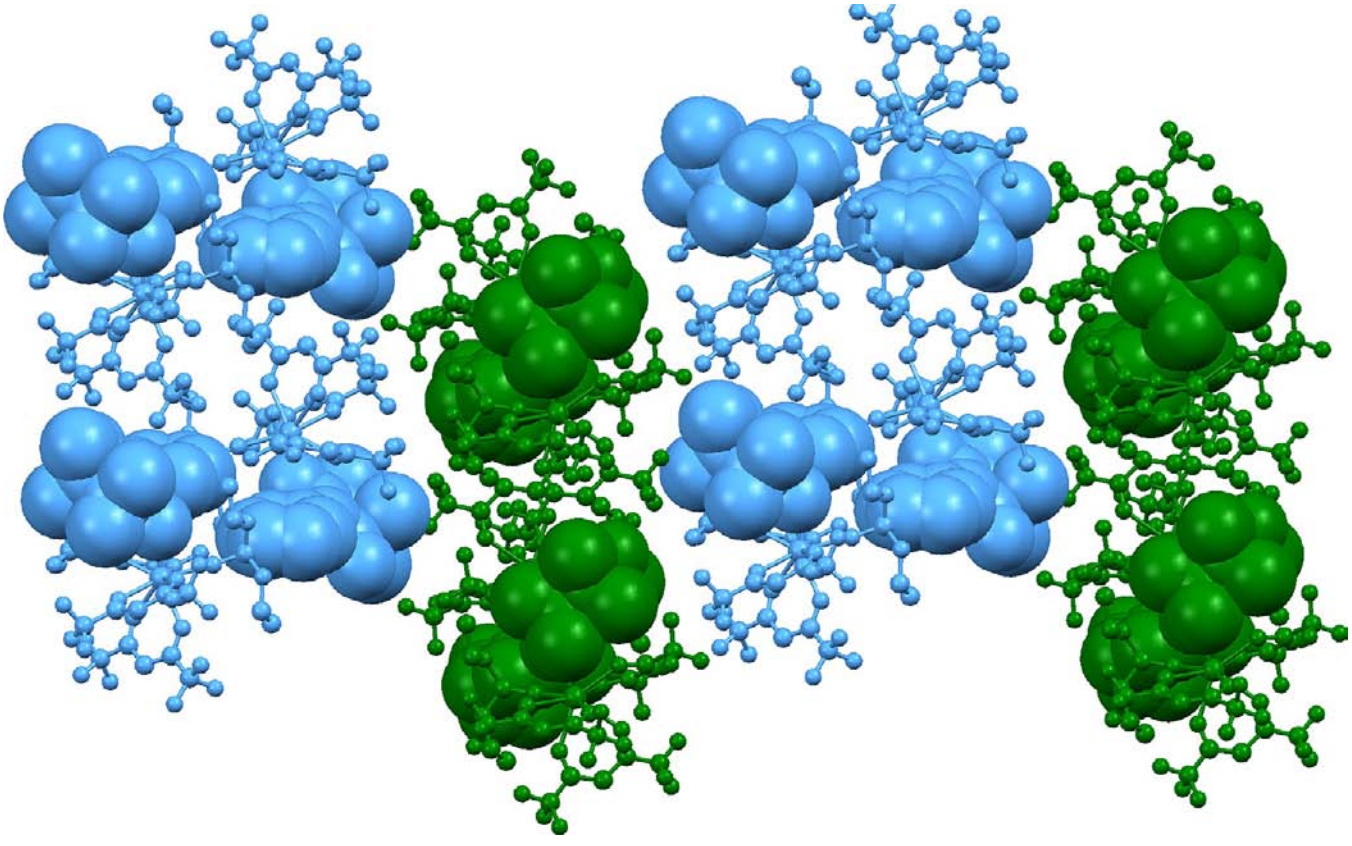

Figure 3. Crystal packing of **2A** showing the arrangement of the well isolated molecules.

dx.doi.org/10.1021/ic301394x | *Inorg. Chem.* 2012, 51, 12218–12229

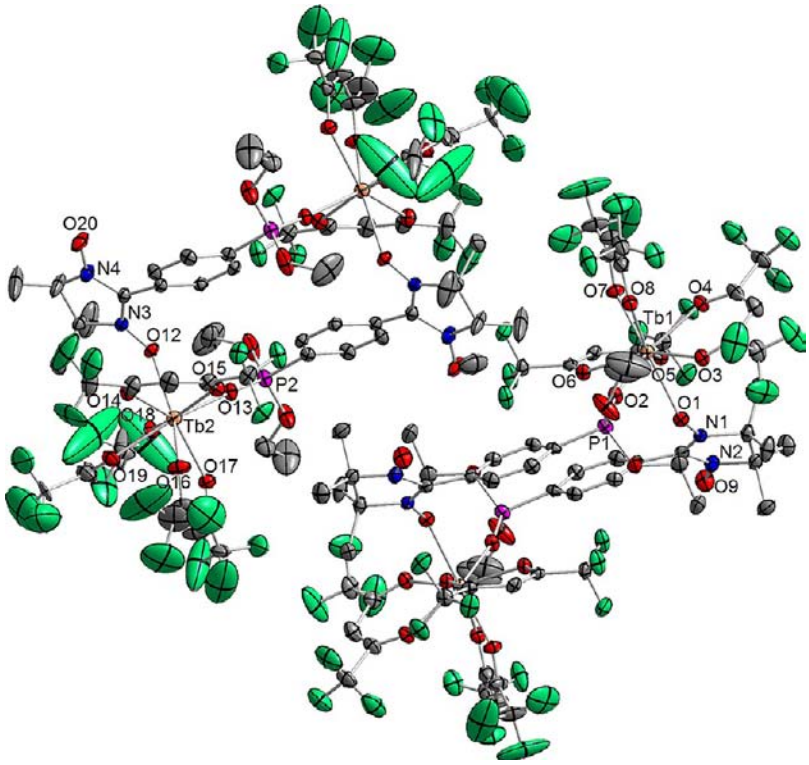

Figure 4. ORTEP view of the molecular structure of **2B** with thermal ellipsoids at 30% probability. Hydrogen atoms are omitted for clarity. Only the three $hfac^-$ ions with the highest occupation factors coordinated to Tb2 are represented.

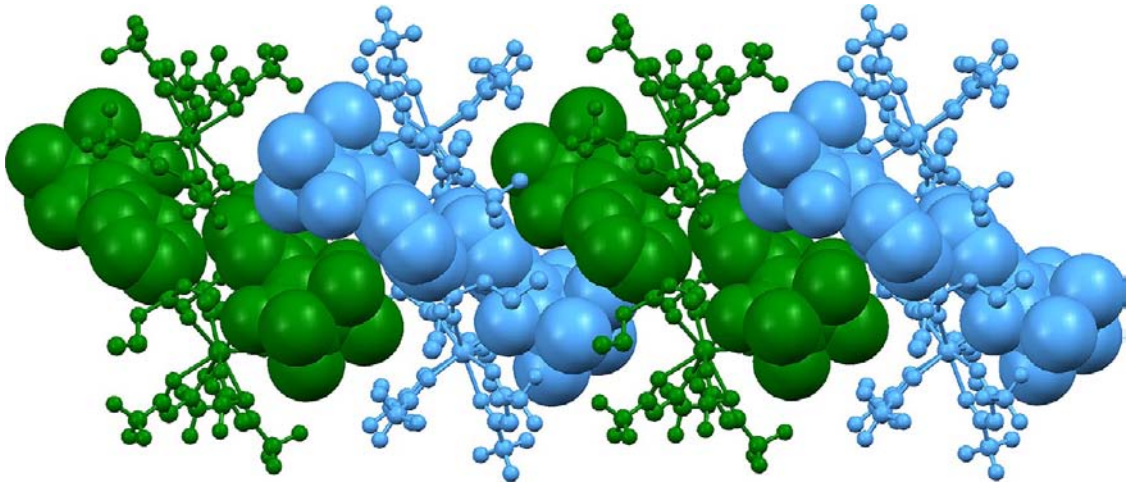

Figure 5. Crystal packing of **2B** showing the short contacts between the neighboring molecular rectangles.

In summary, the reaction between the anhydrous $Ln(hfac)_3$ moieties and the nitronyl nitroxide $NITPhPO(OEt)_2$ gives only magnetically well isolated cyclic dimers for Ln = Gd^{III} **1**, only nonmagnetically isolated cyclic dimers for Ln = Dy^{III} **3**, and a mix of isolated **2A** (about 70%) and nonisolated **2B** (about 30%) cyclic dimers for Ln = Tb^{III} that can be easily separated and analyzed as pure derivatives.

It is expected that the $4f^n$ lanthanides with $n \leq 7$ crystallize in same monoclinic phase as **1**, while the $4f^n$ lanthanides with $n \geq 9$ give the same X-ray structure as **3**.

Static Magnetic Properties. *$[Gd(hfac)_3(NITPhPO(OEt)_2)]_2$ (**1**).* The thermal variation of the $\chi_M T$ product is depicted in Figure 7. At room temperature, $\chi_M T$ takes a value of 16.6 cm^3 K mol^{-1}, which is slightly higher than the expected value for two isolated Gd^{III} ($S = 7/2$) and two radicals ($S = 1/2$) ($\chi_M T$ = 16.5 cm^3 K mol^{-1}). $\chi_M T$ remains almost constant as T is lowered to ca. 100 K. Below this temperature $\chi_M T$ increases to reach 19.95 cm^3 K mol^{-1} at 2.5 K. This indicates that clear ferromagnetic interactions are present in the compound. Compound **1** thus has an $S = 4$ ground state and an $S = 3$ excited state, as seen on many Gd-NIT-R derivatives.[19] Studies on similar rectangular complexes[20,21] suggest that these interactions can occur through different pathways. A strong ferromagnetic interaction is expected between the radical and the directly bound Gd^{III} ion ($J_{Gd\text{-}Rad}$). A smaller one can be transmitted through the whole ligand to reach the Gd^{III} that is on the shorter edge of the rectangle ($J'_{Gd\text{-}Rad}$). For example, on the smaller molecular rectangle of formula $[Gd(hfac)_3(NITpPy)]_2$,[20] the strongest

dx.doi.org/10.1021/ic301394x | *Inorg. Chem.* 2012, 51, 12218−12229

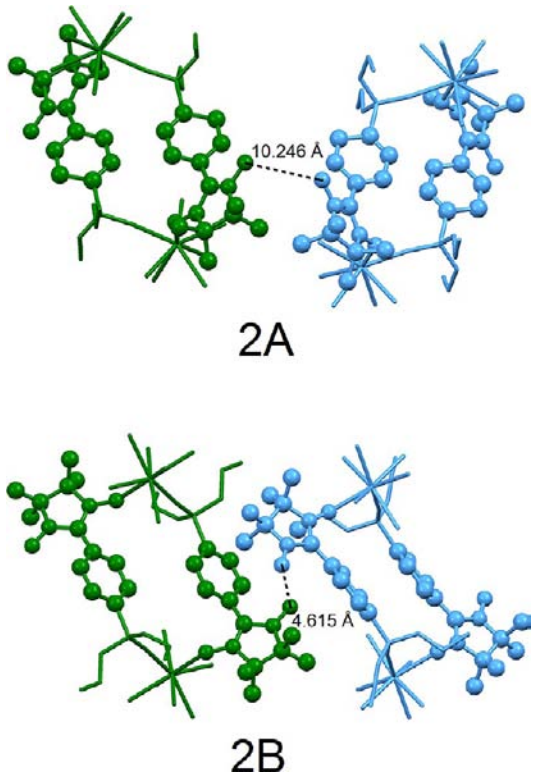

Figure 6. Shortest intermolecular distances between two N−O radicals of neighboring molecules.

interaction is J = 1.78 cm^{-1} and the smallest (through the nitrogen atom of the pyridine ring) is J' = 0.17 cm^{-1}. This leads to a value of $\chi_M T$ at low temperatures (1.6 K) higher than the maximum value for two isolated S = 4 systems. On **1**, the maximum value of $\chi_M T$ at 3 K corresponds to the expected value for two isolated Gd-radical pairs (20 cm^3 K mol^{-1}), and no extra J' interaction is expected. In fact, the large length of the NITPhPO(OEt)$_2$ ligand avoids the transmission of any magnetic exchange interaction ($J'_{\text{Gd-Rad}}$) between the radical and the opposite Gd^{III} ion. Hence, from the magnetic point of view, the molecular rectangle **1** can be described as two isolated Gd(III)−radical pairs. Using $H = -JS_{Gd}\cdot S_{rad}$ as the interaction Hamiltonian provides a septet−nonet energy gap of $4J$ and a theoretical expression for $\chi_M T$ like $\chi_M T = (4N\beta^2 g^2/k)((30 + 14\exp(-4J/kT))/(9 + 7\exp(-4J/kT))$,[22] where N is the Avogadro constant, β is Bohr's magneton, k is Boltzmann's constant, and g is the Landé factor of both radicals and metal centers. The best fit R = 0.995 is shown in Figure 7, and $J_{\text{Gd-Rad}}$ is found to be equal to 3.46 ± 0.04 cm^{-1} with $g_{Gd} = g_{Rad}$ = 2.00. It can be noted that no reliable fit has been obtained considering an extra $J'_{\text{Gd-Rad}}$, confirming that the Gd−radical pairs are isolated. In **1**, $J_{\text{Gd-Rad}}$ is stronger than in [Gd(hfac)$_3$(NITpPy)]$_2$. This may be due to the different nature of the radical ligand leading to different Gd−O1−N1 angles (138.0° for [Gd(hfac)$_3$(NITpPy)]$_2$ versus 131.0° for our compound). This variation could lead to a change of the overlap of the magnetic π^* orbital of the radical with the empty 6s orbital of the Gd^{III} ion, transferring there some unpaired spin density and polarizing the spins of the seven electrons in the 4f orbitals.[23] The experimental and calculated magnetization of **1** is depicted in the inset of Figure 7. The calculated magnetization is obtained from a classical Brillouin function for two uncorrelated S = 7/2 and S = 1/2. The value of the magnetization is 15 μ_B at 6 T and is close to the expected saturated value of 16 μ_B for two Gd^{III} (S = 7/2) ions and two radical ligands (S = 1/2). For any field, the calculated magnetization is lower than the experimental one. This confirms the ferromagnetic exchange interaction between the Gd^{III} ion and the nitronyl nitroxide radical. A second molecular rectangle of formula [Mn(hfac)$_2$(pPONIT)]$_2$ reported by Kahn et al.[16] can be considered to perform a good comparison on the J' interaction. In this compound, a very weak J' antiferromagnetic exchange interaction is reported with a magnetic

Table 1. Crystallographic Data for [Gd(hfac)$_3$(NITPhPO(OEt)$_2$)]$_2$ (1), [Tb(hfac)$_3$(NITPhPO(OEt)$_2$)]$_2$ (2A and 2B), and [Dy(hfac)$_3$(NITPhPO(OEt)$_2$)]$_2$ (3)

compound	**1**	**2A**·2CH$_2$Cl$_2$	**2B**	**3**
formula	$C_{64}H_{58}N_4O_{22}F_{36}P_2Gd_2$	$C_{66}H_{62}N_4Cl_4O_{22}F_{36}P_2Tb_2$	$C_{64}H_{58}N_4O_{22}F_{36}P_2Tb_2$	$C_{64}H_{58}N_4O_{22}F_{36}P_2Dy_2$
M/g mol^{-1}	2295.7	2469.0	2299.0	2306.2
cryst syst	monoclinic	monoclinic	triclinic	triclinic
space group	$P2_1/n$ (No. 14)	$P2_1/n$ (No. 14)	$P\bar{1}$(No. 2)	$P\bar{1}$ (No. 2)
cell parameters	a = 12.1997(10) Å	a = 12.1688(9) Å	a = 12.6405(8) Å	a = 12.6338(3) Å
	b = 16.2486(17) Å	b = 22.7303(17) Å	b = 18.8158(12) Å	b = 18.8107(5) Å
	c = 22.6444(24) Å	c = 16.4500(12) Å,	c = 20.4054(13) Å,	c = 20.4124(5) Å,
	α = 90°	α = 90°	α = 102.9512(23)°	α = 103.0003(12)°
	β = 99.3007(51)°	β = 90.6503(31)°	β = 104.6762(22)°	β = 104.4781(12)°
	γ = 90°	γ = 90°	γ = 105.1194(22)°	γ = 105.2316(12)°
volume/Å^3	4429.7(8)	4549.8(6)	4308.0(5)	4307.1(3)
cell formula units	Z = 4	Z = 4	Z = 2	Z = 2
T/K	150 (2)	150 (2)	150 (2)	150 (2)
diffraction reflection	5.92° ≤ 2θ ≤ 54.96°	3.06° ≤ 2θ ≤ 55.28°	2.18° ≤ 2θ ≤ 55.20°	4.50° ≤ 2θ ≤ 54.84°
ρ_{calcd}, Mg/m^3	1.721	1.802	1.772	1.778
μ, mm^{-1}	1.663	1.836	1.812	1.906
number of reflns	36001	33489	66183	66998
independent reflns	10069	10372	19387	19219
$F_o > 4\sigma(F_o)$	6819	6877	14163	14869
number of variables	599	620	1236	1250
R_{int}, R_1, wR_2	0.0967, 0.1208, 0.2919	0.0810, 0.0658, 0.1770	0.0409, 0.0546, 0.1351	0.0299, 0.0429, 0.1141

dx.doi.org/10.1021/ic301394x | Inorg. Chem. 2012, 51, 12218−12229

Table 2. Selected Bond Lengths (Å) and Angles (deg) for 1, 2A, 2B, and 3

1		2A		2B		3	
Gd1–O1	2.378(8)	Tb1–O1	2.366(6)	Tb1–O1	2.396(4)	Tb2–O12	2.358(5)	Dy1–O1	2.387(4)	Dy2–O12	2.347(4)
Gd1–O2	2.333(9)	Tb1–O2	2.296(5)	Tb1–O2	2.301(4)	Tb2–O13	2.307(4)	Dy1–O2	2.292(4)	Dy2–O13	2.296(4)
Gd1–O3	2.383(9)	Tb1–O3	2.411(6)	Tb1–O3	2.414(4)	Tb2–O14	2.373(5)	Dy1–O3	2.345(3)	Dy2–O14	2.360(4)
Gd1–O4	2.406(9)	Tb1–O4	2.369(6)	Tb1–O4	2.341(5)	Tb2–O15	2.385(5)	Dy1–O4	2.374(4)	Dy2–O15	2.371(4)
Gd1–O5	2.405(9)	Tb1–O5	2.417(6)	Tb1–O5	2.357(4)	Tb2–O16	2.367(5)	Dy1–O5	2.373(4)	Dy2–O16	2.373(4)
Gd1–O6	2.377(9)	Tb1–O6	2.367(6)	Tb1–O6	2.388(4)	Tb2–O17	2.379(5)	Dy1–O6	2.356(4)	Dy2–O17	2.359(5)
Gd1–O7	2.356(9)	Tb1–O7	2.366(6)	Tb1–O7	2.380(5)	Tb2–O18	2.395(5)	Dy1–O7	2.332(4)	Dy2–O18	2.386(4)
Gd1–O8	2.433(12)	Tb1–O8	2.385(6)	Tb1–O8	2.364(5)	Tb2–O19	2.365(6)	Dy1–O8	2.401(4)	Dy2–O19	2.342(4)
N1–O1	1.298(16)	N1–O1	1.337(9)	N1–O1	1.309(7)	N3–O12	1.307(7)	N1–O1	1.311(6)	N3–O12	1.304(5)
N2–O9	1.270(20)	N2–O9	1.294(9)	N2–O9	1.272(8)	N4–O20	1.266(8)	N2–O9	1.281(7)	N4–O20	1.269(6)
P1–O2	1.450(10)	P1–O2	1.491(6)	P1–O2	1.472(5)	P2–O13	1.470(5)	P1–O2	1.470(4)	P2–O13	1.472(4)
Gd1–O1–N1	131.4(9)	Tb1–O1–N1	131.8(5)	Tb1–O1–N1	133.0(3)	Tb2–O12–N3	135.4(4)	Dy1–O1–N1	133.2(3)	Dy2–O12–N3	135.9(3)
Gd1–O2–P1	167.0(7)	Tb1–O2–P1	164.8(4)	Tb1–O2–P1	166.8(3)	Tb2–O13–P2	172.1(3)	Dy1–O2–P1	166.5(2)	Dy2–O13–P2	171.6(2)
O1–Gd1–O2	79.3(3)	O1–Tb1–O2	81.1(2)	O1–Tb1–O2	76.93(16)	O12–Tb2–O13	75.98(16)	O1–Dy1–O2	77.09(13)	O12–Dy2–O13	76.26(13)
O3–Gd1–O4	72.3(3)	O3–Tb1–O4	70.9(2)	O3–Tb1–O4	70.71(16)	O14–Tb2–O15	72.27(16)	O3–Dy1–O4	72.18(12)	O14–Dy2–O15	72.41(13)
O5–Gd1–O6	70.1(3)	O5–Tb1–O6	69.8(2)	O5–Tb1–O6	71.84(14)	O16–Tb2–O17	70.05(18)	O5–Dy1–O6	70.58(14)	O16–Dy2–O17	70.22(16)
O7–Gd1–O8	70.8(4)	O7–Tb1–O8	72.6(2)	O7–Tb1–O8	70.26(17)	O18–Tb2–O19	70.00(19)	O7–Dy1–O8	71.17(14)	O18–Dy2–O19	70.15(15)

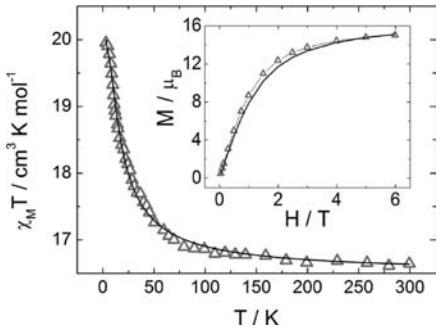

Figure 7. Temperature dependence of the $\chi_M T$ product for **1** (triangles) and best fit (full black line) in 2.5−300 K temperature range measured with 0.1 T dc field. In the inset, experimental (triangle) and calculated for uncorrelated spin system (full black line) magnetization of **1**, at 2.5 K in 0−6 T field range.

exchange interaction of −0.03 cm^{-1}. The origin of this interaction could not be unambiguously determined from the data. It can be either of an intramolecular nature (mediated by the ligand via the P═O bond) or intermolecular. Anyway, it is well-known that in the case of 4f ions the magnetic 2p−4f interaction is weaker than with 3d ions; hence, our assumption of a negligible J' exchange interaction seems to be pertinent.

*[(Tb(hfac)$_3$(NITPhPO(OEt)$_2$)]$_2$ (**2A** and **2B**).* The temperature dependence of the molar magnetic susceptibilities χ_M of **2A** and **2B** are shown in Figure 8 as a plot of $\chi_M T$ vs T. At 300

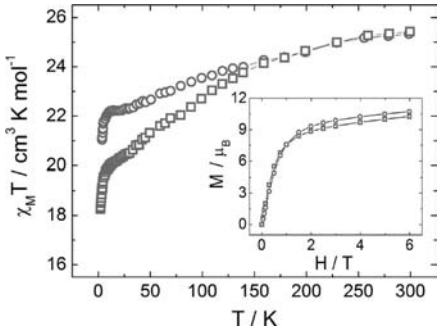

Figure 8. Temperature dependence of $\chi_M T$ for **2A** (circles) and **2B** (squares) measured with a 0.05 T dc field from 2.5 to 250 K and 0.1 T above. Inset: experimental magnetization of **2A** (circles) and **2B** (squares) at 2.5 K in the 0−6 T field range.

K, the $\chi_M T$ product takes a value of 25.3 cm^3 K mol^{-1} for **2A** and 25.4 cm^3 K mol^{-1} for **2B**. These values are slightly higher than the expected value of 24.4 cm^3 K mol^{-1} for two Tb^{III} ions and two nitronyl nitroxide radicals (S = 1/2, g = 2.00) taken as isolated. Both complexes show a decrease of $\chi_M T$ on lowering the temperature, and at 30 K a slope change is observed. For **2A**, in the 30−9 K temperature range, the $\chi_M T$ product takes a quasi constant value of 22.2 cm^3 K mol^{-1}, whereas for **2B**, it decreases slowly from 20.5 cm^3 K mol^{-1} to 19.9 cm^3 K mol^{-1}. Below 9 K, the $\chi_M T$ product of both curves decreases abruptly to reach 21.0 cm^3 K mol^{-1} and 18.3 cm^3 K mol^{-1} at 2.5 K for **2A** and **2B**, respectively. The experimental magnetization of **2A** and **2B** is shown in the inset of Figure 8. At 6 T, the magnetization values of **2A** and **2B** are 11.3 μ_B and 10.3 μ_B, respectively. These are lower than the expected saturated value of 20 μ_B for two Tb^{III} ions and two radicals.

The ground state of a Tb^{III} ion (electronic configuration $4f^8$) is $^7F_6$ characterized by g_J = 3/2.[19] The first excited state ($^7F_5$) is

dx.doi.org/10.1021/ic301394x | Inorg. Chem. 2012, 51, 12218−12229

separated by 2000 cm^{-1} from the ground state.[22] When the temperature decreases, the $\chi_M T$ (T) curve decreases because of the progressive depopulation of the $J = 6$ multiplet of the Tb^{III} even in the absence of any exchange interaction.[24] From 300 K to 30 K, the decrease of the $\chi_M T$ product for both dinuclear complexes is therefore principally attributed to the depopulation of the M_J states of the two Tb^{III} ions. This depopulation strongly depends on the coordination sphere symmetry, and so, we may attribute the difference of decreasing between 150 and 50 K to the difference of geometry around the Tb^{III} ions in **2A** and **2B** (values in synthesis and structure description section). Below 50 K, this phenomenon is still present but can be combined with others. For example, the slope change below 50 K can be a consequence of a ferromagnetic exchange interaction between the radical ($S = 1/2$) and the Tb^{III} ion as seen on the Gd^{III} derivative (**1**). In the same way, below 9 K, the $\chi_M T$ evolution can be due also to intermolecular antiferromagnetic exchange interactions if present. This must be the cause of the low temperature discrepancies between $\chi_M T$ vs T curves of **2A** and **2B** as their crystal packing is different. As stated before, the N−O groups are known to transmit through space magnetic interaction provided they are not too far.[20,21,25,7g] A close examination of the distance and angles between those N−O groups confirms that this interaction should be antiferromagnetic in nature.[25]

This antiferromagnetic interaction in **2B** is confirmed by the M vs H curves (inset of Figure 8) where for any field, the experimental magnetization of **2B** is lower than the one of **2A**. If one takes into account that the intramolecular ferromagnetic exchange interactions are equal in both compounds **2A** and **2B**, the observation of the magnetization behavior confirms the existence of intermolecular antiferromagnetic exchange interaction in **2B**.

*$[(Dy(hfac)_3(NITPhPO(OEt)_2)]_2$ (**3**).* The temperature dependence of the molar magnetic susceptibility χ_M of **3** is shown in Figure S3 as a plot of $\chi_M T$ vs T. At 300 K, $\chi_M T$ takes a value of 29.6 cm^3 K mol^{-1}. This value is slightly higher than the expected value of 29.1 cm^3 K mol^{-1} for two Dy^{III} ions and two nitronyl nitroxide radicals ($S = 1/2$, $g = 2.00$). It then decreases continuously to reach 19.2 cm^3 K mol^{-1} at 2.5 K. The experimental magnetization of **3** is depicted in the inset of Figure S3. At 6 T, the magnetization is 16.3 μ_B, lower than the expected saturated value of 22 μ_B for two Dy^{III} ions and two radicals.

Compound **3** is iso-structural to **2B**, but contrary to this one, no change in the slope of $\chi_M T$ vs T is observed. Moreover, in the previously reported $[Dy(hfac)_3(NITpPy)]_2$ rectangle, a ferromagnetic exchange interaction has been found through the N−O group bonded to the dysprosium ion.[10] Anyway, in **3**, this supposed ferromagnetic exchange interaction is not observed because of the addition of three possible phenomena: (1) the crystal field effect on the Dy^{III} ion, (2) the intermolecular antiferromagnetic interaction since the compound is isostructural to **2B**, and (3) ferromagnetic exchange interactions that are supposed to be weaker in **3** than in the Tb derivatives (**2A** and **2B**).

Dynamic Magnetic Properties. *$[(Dy(hfac)_3(NITPhPO(OEt)_2)]_2$ (**3**).* Our dynamic magnetic investigation has focused first on the Dy^{III} derivative, this lanthanide cation featuring a great ability to show magnetic slow relaxation.[5−7] Surprisingly, no frequency dependence of the dynamic susceptibility has been observed. This is possibly a consequence of the environment of the Dy^{III} ion that can lead (i) to a small separation of the ground and excited states and thus to fast relaxation and (ii) to a stabilization of M_J states, which does not permit slow relaxation of the magnetization.

*$[(Tb(hfac)_3(NITPhPO(OEt)_2)]_2$ (**2B**).* The dynamic properties of the magnetization of the most close-packed form of the Tb derivative, **2B**, have been investigated. In zero field, a very weak frequency dependence of the susceptibility is observed (Figures 9 and S4), and a reliable extraction of dynamic parameters is

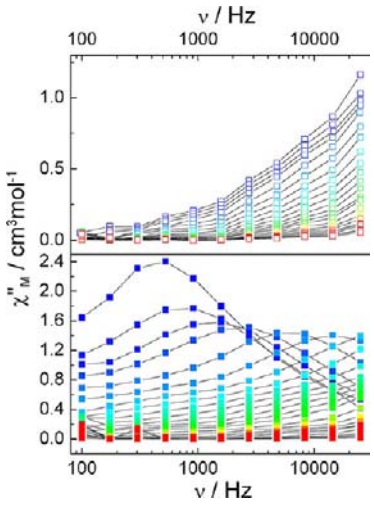

Figure 9. Frequency dependence of χ_M'' for **2B**, measured from 1.8 K (blue) to 6 K (red) in zero (top) and 0.2 T static field (bottom). Measurements were taken from 1.8 to 2 K, 2.2 to 4 K, and 4.4 to 6 K with 0.1, 0.2, and 0.4 K spacing respectively. Lines are guides to the eye.

impossible. This can be a consequence of zero-field fast tunnelling[5c,26] that is reported to be cancellable by the application of a small external static field.[5g,27]

The field dependence of χ_M'' has been thus measured at 2 K (Figure S5). Frequency dependence is observed and a 0.2 T field is then chosen for in-field dynamic measurements. Clear frequency dependence is now visible from 1.7 to 2.6 K, and the χ_M'' vs frequency curves have been fitted according to an extended Debye model (Table S1). The characteristic dynamic parameters have been plotted considering an Arrhenius law ($\tau = \tau_0 \exp(\Delta/T)$ where τ_o is the characteristic relaxation time and Δ is the activation energy for the process. For **2B**, extracted values are $\tau_o = (1.76 \pm 0.20) \times 10^{-9}$ s and $\Delta = 21.0 \pm 0.5$ K ($R = 0.997$; Figure 10). These relaxation rates are comparable with the values of the literature for tetranuclear compounds Cu_2Tb_2 ($\Delta = 21$ K, $\tau_o = 2.7 \times 10^{-8}$ s,[4b] $\Delta = 4.2$ K, $\tau_o = 1 \times 10^{-5}$ s,[28] and $\Delta = 4.2$ K, $\tau_o = 1 \times 10^{-5}$ s,[7h]) and for the dinuclear compound CuTb ($\Delta = 28.5$ K, $\tau_o = 3.8 \times 10^{-5}$ s).[29] The distribution of the relaxation times can be studied by plotting χ_M'' vs χ_M' in a so-called Argand plot. The resulting curves can be fitted using the Debye model with

$$\chi(\omega) = \chi_S + \frac{\chi_T - \chi_S}{1 + (i\omega\tau)^{1-\alpha}}$$

in which $\chi_T = \chi(\omega \rightarrow 0)$ is the isothermal susceptibility and $\chi_s = \chi(\omega \rightarrow \infty)$ is the adiabatic susceptibility, ω being the angular frequency of the ac field and τ being the relaxation time of the system at the temperature of the measurement.[30] The α parameter is introduced in the Debye law to characterize the distribution of the relaxation times:[30,31] $\alpha = 0$ corresponds to a

dx.doi.org/10.1021/ic301394x | Inorg. Chem. 2012, 51, 12218−12229

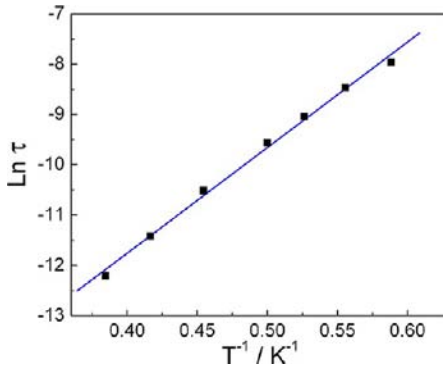

Figure 10. Arrhenius plots of the relaxation times extracted from the in-field measurements with the best linear fit (see text for values) for **2B**.

unique relaxation time and is thus expected for an ideal SMM.[32] On the contrary, $\alpha \rightarrow 1$ corresponds to an infinity of relaxation times and is characteristic of spin-glasses.[33] For **2B** distribution of the relaxation times, α is almost constant at 0.33 along the whole relaxing temperature range (1.7−2.6 K; Table S1).

*[(Tb(hfac)$_3$(NITPhPO(OEt)$_2$)]$_2$ (**2A**).* Also in this case the in-phase (χ_M') and out-of-phase (χ_M'') components of the magnetic susceptibility were measured in zero static field. The χ_M'' vs frequency curve shows a complex behavior with a set of temperature dependent peaks from 5 to 3 K and a temperature independent one at lower temperatures (Figure 11

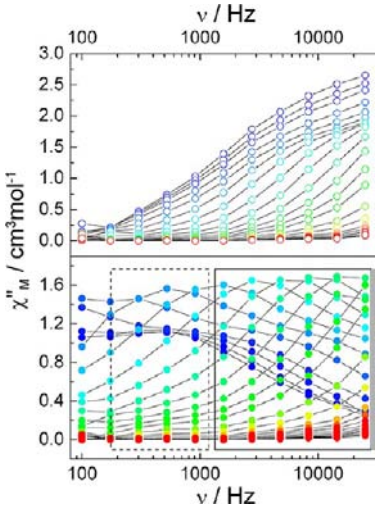

Figure 11. Frequency dependence of χ_M'' for **2A**, measured from 1.8 K (blue) to 6 K (red) in a zero (top) and 0.2 T static field (bottom) with the two different relaxation mechanisms highlighted with dashed (frequency independent) and full (frequency dependent) square. Measurements were undertaken from 1.8 to 2 K, 2.2 to 4 K, and 4.4 to 6 K with 0.1, 0.2, and 0.4 K spacing, respectively. Lines are guides to the eye.

and S6). For $T > 3$ K the energy barrier is estimated at 24 ± 1 K for a characteristic relaxation time of $\tau_0 = 3.36 \pm 0.40 \times 10^{-9}$ s. A transition is observed below 3 K as the energy barrier vanishes and the complex relaxes through an under barrier mechanism with a tunnelling rate estimated at 7500 ± 20 Hz (Table S2).

In order to better understand these dynamic features, the field dependence of χ_M'' has been measured at 2 K. In the absence of field, **2A** presents a very fast relaxation. However, a small field (0.05 T) is enough to remove the quantum tunnelling (QT) and promote a slower mechanism. The relaxation rate is so slow that it shifts out of our investigation range (100−25000 Hz) at 2 K (Figure S7). To allow comparison with **2B**, we then chose a field of 0.2 T to investigate the in-field temperature dependence of χ_M''. The in-field χ_M'' vs frequency curves show that the two relaxation regimes (thermally and nonthermally activated) are present at each temperature (Figure S8). At high temperatures, the thermally activated regime prevails but the curves can be fitted considering that the QT regime slightly contributes to the relaxation. Reciprocally, some features of the thermally activated relaxation regime are present at low temperatures, whereas the QT is prominent. The relaxation rates (τ) have thus been extracted considering a double relaxation process, and the τ's that belong to the nonpredominant regime have been reported as gray-filled circles in the Arrhenius plot (Figure 12, Table S3). The energy barrier for the high temperature

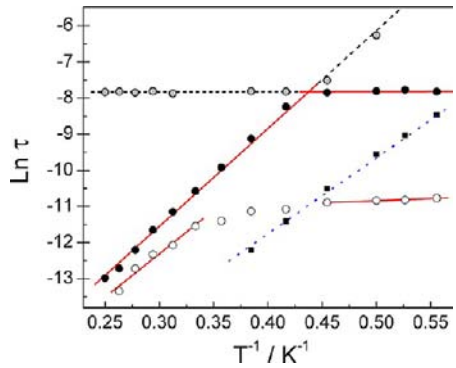

Figure 12. Arrhenius plots of the relaxation times extracted from the zero-field (empty black circles) and in-field (full black circles) measurements with the best linear fits (see text for values) for **2A**. Gray filled circles stand for the relaxation times extracted from the residual peaks of the χ_M'' vs frequency curves. Arrhenius plot of the relaxation times extracted from in-field (squares) measurements and its best fit (dashed blue line) for **2B** is reported for comparison.

regime is comparable to the previous one with 27.50 ± 0.60 K and a characteristic relaxation time of $\tau_0 = 2.64 \pm 0.25 \times 10^{-9}$ s. The tunnelling rate is 20 times slower with 400 ± 5 Hz. The presence of mixed relaxation processes is expected to impact the distribution of the relaxation times. The Argand plot clearly evidences this as the χ_M'' vs χ_M' curves can be fitted with a single α parameter only in narrow temperature ranges, i.e., at the extremes of the temperature range where the contribution of the minor relaxation process is negligible (Figure 13). At 1.8 K, $\alpha = 0.38$, $\chi_S = 0.7$ and $\chi_T = 5.05$ cm^3 mol^{-1} ($R^2 = 0.9997$). At 3 K, $\alpha = 0.28$, $\chi_S = 1.48$, and $\chi_T = 6.78$ cm^3 mol^{-1} ($R^2 = 0.9995$). The mixed relaxation processes are highlighted here by the high χ_S value of this second regime, where a significant part of the system can still relax according to the low temperature regime (i.e., QT). In between these extremes, a double relaxation process has to be considered for each temperature, and so two different α values are used (Figure S9, Table S3). The dynamic relaxation figures of **2A** and **2B** are gathered in Table 3 for comparison. All extracted parameters are similar, with τ_o ranging from 1.76 to 3.36 × 10^{-9} s and Δ from 21 to 27.5 K. The 0.2 T external field reveals for both complexes a similar magnetic behavior that is thus supposed to be intrinsic of the complex. Compound **2A** has a crystal packing that

dx.doi.org/10.1021/ic301394x | *Inorg. Chem.* 2012, 51, 12218−12229

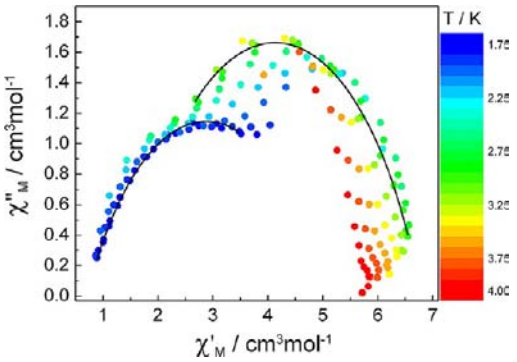

Figure 13. Argand plot for **2A** with best fits for the low (1.8 K) and the high temperature (3 K) regions.

provides a good insulation of the complexes, and thus slow relaxation is observed with or without external field with QT at low temperatures in both cases. The close-packed derivative (**2B**) presents intermolecular magnetic interactions that affect its dynamic magnetic properties. In zero field, the QT is so fast that it is not measurable with our instrument (i.e., > 25 000 Hz). In **2B**, the dimers are organized into a 1D structure, and a small intermolecular magnetic interaction is expected. However, this interaction is not strong enough to permit the creation of a correlation length at low T as observed on SCMs.[34] This explains why, and contrary to what was observed on other 1D SMM organizations,[35] the dimers organized into a 1D structure (**2B**) relax faster than isolated dimers (**2A**). With a 0.2 T field, the SMM behavior of **2B** shifts toward lower temperatures, and only part of it is visible in our investigation range (T > 1.6 K). The applied field seems to affect only the dimers, and interplay with the intermolecular magnetic interactions can be ruled out. In fact, isolated dimers (**2A**) that are not expected to present any intermolecular magnetic interactions are also highly field sensitive.

The two derivatives show the same intrinsic behavior, but the poor magnetic insulation of **2B** shifts the "observation window" of the SMM behavior toward highest frequencies and lower temperatures.

CONCLUSIONS

The synthesis and structures of four new cyclic dinuclear compounds involving nitronyl nitroxide as radical ligands are reported. The crystal packing of the $[Ln(hfac)_3(NITPhPO(OEt)_2)]_2$ (Ln = Gd^{III} (**1**), Tb^{III} (**2A** and **2B**), and Dy^{III} (**3**)) compounds depends on the trend of the lanthanide ionic radius along the series with a coexistence of both crystal packings in the case of the Tb^{III} derivative. In **2A**, the molecules are well-isolated, whereas in **2B** they interact through short contacts between the N−O groups. Static magnetic studies show that lanthanides and radicals are ferromagnetically coupled. In the case of the isotropic Gd^{III} derivative, the magnetic exchange interaction has been evaluated to J = 3.46 cm^{-1} ± 0.04 cm^{-1}. While compound **3** does not show any out-of-phase signal, both compounds **2A** and **2B** exhibit SMM behavior. Compound **2B** shows a thermally activated regime with pre-exponential factors of 1.76 ± 0.20 × 10^{-9} s and energy barriers of 21 K under an applied external magnetic field. In the well-isolated form (**2A**), the thermally activated regime is observed in both zero and 0.2 T applied external magnetic field (τ_0 = 3.36 × 10^{-9} and 2.64 × 10^{-9} s, and Δ = 24.0 and 27.5 K, respectively). The good magnetic insulation of the complexes in **2A** allows the observation of the SMM behavior of the molecular rectangles in an "observation window" centered at higher temperatures and slower frequencies.

Very recently, the influence of the β-diketonate ancillary ligands on the dynamic magnetic properties of similar Tb^{III} based molecular rectangles has been evidenced. An optimization of the SMM properties is possible by an appropriate choice of the crystal that is supposed to influence the ligand-field strength of the lanthanide and so the SMM behavior of the complexes.[7h] We show here that a similar optimization can be done by carefully insulating the molecular rectangles. The combination of the two approaches can possibly lead to advances in the design of high temperature relaxing Tb-radical based SMMs.

It is worth notice that the number of metal-radical-based systems is small over the large amount of reported SMMs. Moreover, in this small class of SMMs, Tb derivatives are found to be the most efficient as well as when they are combined with S = 1/2 spins (Cu^{II}, noninnocent organic ligands). This is in contradiction to what is currently observed in lanthanide-based SMMs that involve nonmagnetic ligands and where Dy^{III} derivatives always offer the richest magnetic behavior. Efforts in the design of Tb^{III} associated to S = 1/2 molecules could lead to better understanding of the relaxation mechanism of lanthanide-based SMMs and provide new and exciting SMMs.

ASSOCIATED CONTENT

Supporting Information

ORTEP views of **1** (Figure S1) and **3** (Figure S2). Thermal dependence of the $\chi_M T$ product and first magnetization of **3** (Figure S3). Field and temperature dependences of the out-of phase χ_M'' for **2A** and **2B** (Figures S4−S7). Frequency dependence at 2.4 K (Figure S8) and Argand diagram (Figure S9) for **2A**. Dynamic parameters for **2A** and **2B** (Tables S1−S3), as well as a CIF file. This material is available free of charge via the Internet at http://pubs.acs.org.

AUTHOR INFORMATION

Corresponding Author

*E-mail: Fabrice.pointillart@univ-rennes1.fr.

Notes

The authors declare no competing financial interest.

Table 3. Dynamic Parameters Extracted for 2A and 2B

compound	H (T)	τ_o (s)		Δ (K)	
2B	0	n.a.		n.a.	
	0.2	1.76 ± 0.20 × 10^{-9}		21.0 ± 0.5	
2A		τ_o (s) HT	Δ (K) HT	τ_o (s) LT	Δ (K) LT
	0	3.36 ± 0.40 × 10^{-9}	24 ± 1	2.1 ± 0.1 × 10^{-5} (7500 Hz)	0
	0.2	2.64 ± 0.25 × 10^{-9}	27.5 ± 0.6	4.0 ± 0.1 × 10^{-4} (400 Hz)	0

dx.doi.org/10.1021/ic301394x | Inorg. Chem. 2012, 51, 12218−12229

■ ACKNOWLEDGMENTS

We acknowledge financial support from Italian MURST (FIRB and PRIN grants), from the EC through the Human Potential Program RTN-QUELMOLNA (MRTN-CT-2003-504880), and from the NE-MAG-MANET (NMP3-CT-2005-515767), and F.P. thanks German DFG (SPP1137) for his postdoctoral fellowship. T. Roisnel is acknowledged for assistance in crystallographic diffraction.

■ REFERENCES

(1) (a) Lis, T. *Acta Crystallogr., Sect. B* **1980**, *36*, 2042. (b) Sessoli, R.; Tsai, H. L.; Schake, A. R.; Wang, S.; Vincent, J. B.; Folting, K.; Gatteschi, D.; Christou, G.; Hendrickson, D. N. *J. Am. Chem. Soc.* **1993**, *115*, 1804. (c) Christou, G.; Gatteschi, D.; Hendrickson, D. N.; Sessoli, R. *MRS Bull.* **2000**, *25*, 66.

(2) (a) Zhang, Y.-Z.; Wernsdorfer, W.; Pan, F.; Wang, Z.-M.; Gao, S. *Chem. Commun.* **2006**, 3302. (b) Yang, E. C.; Hendrickson, D. N.; Wernsdorfer, W.; Nakano, M.; Zaharov, L. N.; Sammer, R. D.; Rheingold, A. L.; Ledezma-Gairaud, M.; Christou, G. *J. Appl. Phys.* **2002**, *91*, 7382. (c) Murrie, M.; Teat, S. J.; Stoeckli-Evans, H.; Güdel, H. U. *Angew. Chem., Int. Ed.* **2003**, *42*, 4653. (d) Langley, S. J.; Helliwell, M.; Sessoli, R.; Rosa, P.; Wernsdorfer, W.; Winpenny, R. E. P. *Chem. Commun.* **2005**, 5029. (e) Chibotaru, L. F.; Ungur, L.; Aronica, C.; Elmoll, H.; Pilet, G.; Luneau, D. *J. Am. Chem. Soc.* **2008**, *130*, 12445.

(3) (a) Stamatatos, T. C.; Abboud, K. A.; Wernsdorfer, W.; Christou, G. *Angew. Chem., Int. Ed.* **2007**, *46*, 884. (b) Ge, C.-H.; Cui, A.-L.; Ni, Z.-H.; Jiang, Y.-B.; Zang, L.-F.; Ribas, J.; Kou, H.-Z. *Inorg. Chem.* **2006**, *45*, 4883. (c) Li, Y.; Wernsdorfer, W.; Clérac, R.; Hewitt, I. J.; Anson, C. E.; Powell, A. K. *Inorg. Chem.* **2006**, *45*, 2376. (d) Lecren, L.; Wernsdorfer, W.; Li, Y.-G.; Roubeau, O.; Miyasaka, H.; Clérac, R. *J. Am. Chem. Soc.* **2005**, *127*, 11311. (e) Kachi-Terajima, C.; Miyasaka, H.; Sugiura, K.; Clérac, R.; Nojiri, H. *Inorg. Chem.* **2006**, *45*, 4381. (f) Milios, C. J.; Vinslava, A.; Whittaker, A. G.; Parsons, S.; Wernsdorfer, W.; Christou, G.; Perlepes, S. P.; Brechin, E. K. *Inorg. Chem.* **2006**, *45*, 5272. (g) Aubin, S. M. J.; Wemple, M. W.; Adams, D. M.; Tsai, H.-L.; Christou, G.; Hendrickson, D. N. *J. Am. Chem. Soc.* **1996**, *118*, 7746.

(4) (a) Costes, J.-P.; Dahan, F.; Wernsdorfer, W. *Inorg. Chem.* **2006**, *45*, 5. (b) Osa, S.; Kido, T.; Matsumoto, N.; Re, N.; Pochaba, A.; Mrozinski, J. *J. Am. Chem. Soc.* **2004**, *126*, 420. (c) Novitchi, G.; Costes, J.-P.; Tuchagues, J.-P.; Vendier, L.; Wernsdorfer, W. *New J. Chem.* **2008**, *32*, 197. (d) Costes, J.-P.; Shova, S.; Wernsdorfer, W. *Dalton Trans.* **2008**, 1843. (e) Long, J.; Chamoreau, L.-M.; Marvaud, V. *Dalton Trans.* **2010**, *39*, 2188.

(5) (a) Aronica, C.; Pilet, G.; Chastanet, G.; Wernsdorfer, W.; Jacquot, J.-F.; Luneau, D. *Angew. Chem., Int. Ed.* **2006**, *45*, 4659. (b) Ishikawa, N.; Sugita, M.; Ishikawa, T.; Koshihara, S.; Kaizu, Y. *J. Am. Chem. Soc.* **2003**, *125*, 8694. (c) Ishikawa, N.; Sugita, M.; Wernsdorfer, W. *J. Am. Chem. Soc.* **2005**, *127*, 3650. (d) Mori, F.; Nyuri, T.; Ishida, T.; Nogami, T.; Choi, K.-Y.; Nojiri, H. *J. Am. Chem. Soc.* **2006**, *128*, 1440. (e) Jiang, S.-D.; Wang, B.-W.; Su, G.; Wang, Z.-M.; Gao, S. *Angew. Chem., Int. Ed.* **2010**, *49*, 7448. (f) Li, D.-P.; Wang, T.-W.; Li, C.-H.; Liu, D.-S.; Li, Y.-Z.; You, X.-Z. *Chem. Commun.* **2010**, *46*, 2929. (g) Layfield, R. A.; McDouall, J. J. W.; Sulway, S. A.; Tuna, F.; Collison, D.; Winpenny, R. E. P. *Chem.—Eur. J.* **2010**, *16*, 4442. (h) Lin, P.-H.; Burchell, T. J.; Clérac, R.; Murugesu, M. *Angew. Chem., Int. Ed.* **2008**, *47*, 8848. (i) Xu, G.-F.; Wang, Q. L.; Gamez, P.; Ma, Y.; Clérac, R.; Tang, J.; Yan, S.-P.; Cheng, P.; Liao, D.-Z. *Chem. Commun.* **2010**, *46*, 1506. (j) Tang, J. K.; Hewitt, I.; Madhu, N. T.; Chastanet, G.; Wernsdorfer, W.; Anson, C. E.; Benelli, C.; Sessoli, R.; Powell, A. K. *Angew. Chem., Int. Ed.* **2006**, *45*, 1729. (k) Hewitt, I. J.; Tang, J.; Mahdu, N. Y.; Anson, C. E.; Lan, Y.; Luzon, J.; Etienne, M.; Sessoli, R.; Powell, A. K. *Angew. Chem., Int. Ed.* **2010**, *49*, 6352. (l) Guo, F.-S.; Liu, J.-L.; Leng, J.-D.; Meng, Z.-S.; Lin, Z.-J.; Tong, M.-L.; Gao, S.; Ungur, L.; Chibotaru, L. F. *Chem.—Eur. J.* **2011**, *17*, 2458. (m) Luzon, J.; Bernot, K.; Hewitt, I. J.; Anson, C. E.; Powell, A. K.; Sessoli, R. *Phys. Rev. Lett.* **2008**, *100*, 247205. (n) Chen, Z.; Zhao, B.; Cheng, P.; Zhao, X.-Q.; Shi, W.; Song, Y. *Inorg. Chem.* **2009**, *48*, 3493. (o) Ritchie, C.; Speldrich, M.; Gable, R. W.; Sorace, L.; Kögerler, P.; Boskovic, C. *Inorg. Chem.* **2011**, *50*, 7004. (p) Yan, P.-F.; Lin, P.-H.; Habib, F.; Aharen, T.; Murugesu, M.; Deng, Z.-P.; Li, G.-M.; Sun, W.-B. *Inorg. Chem.* **2011**, *50*, 7059. (q) Pointillart, F.; Bernot, K.; Sessoli, R.; Gatteschi, D. *Inorg. Chem.* **2010**, *49*, 4355. (r) Guo, Y.-N; Xu, G.-F.; Wernsdorfer, W.; Ungur, L.; Tang, J.; Zhang, H.-J.; Chibotaru, L. F.; Powell, A. K. *J. Am. Chem. Soc.* **2011**, *133*, 11948. (s) Tian, H.; Wang, M.; Zhao, L.; Guo, Y. N.; Guo, Y.; Tang, J.; Liu, Z. *Chem.—Eur. J.* **2012**, *18*, 442. (t) Hewitt, I. J.; Lan, Y.; Anson, C. E.; Luzon, J.; Sessoli, R.; Powell, A. K. *Chem. Commun.* **2009**, 6765. (u) Tian, H.; Zhao, L.; Guo, Y.-N.; Guo, Y.; Tang, J.; Liu, Z. *Chem. Commun.* **2012**, *48*, 708.

(6) (a) Tsukuda, T.; Suzuki, T.; Kaizaki, S. *J. Chem. Soc., Dalton Trans.* **2002**, 1721. (b) Lescop, C.; Luneau, D.; Rey, P.; Bussière, G.; Reber, C. *Inorg. Chem.* **2002**, *41*, 5566. (c) Kaizaki, S.; Shirotani, D.; Tsukahara, Y.; Nakata, H. *Eur. J. Inorg. Chem.* **2005**, 3503. (d) Bernot, K.; Luzon, J.; Bogani, L.; Etienne, M.; Sangregorio, C.; Shanmugam, M.; Caneschi, A.; Sessoli, R.; Gatteschi, D. *J. Am. Chem. Soc.* **2009**, *131*, 5573. (e) Xu, J. X.; Ma, Y.; Liao, D. Z.; Xu, G. F.; Tang, J. K.; Wang, C.; Zhou, N.; Yan, S. P.; Cheng, P.; Li, L. C. *Inorg. Chem.* **2009**, *48*, 8890. (f) Tian, H. X.; Liu, R. N.; Wang, X. L.; Yang, P. P.; Li, Z. X.; Li, L. C.; Liao, D. Z. *Eur. J. Inorg. Chem.* **2009**, 4498. (g) Zhou, N.; Ma, Y.; Wang, C.; Xu, G. F.; Tang, J. K.; Xu, J. X.; Yan, S. P.; Cheng, P.; Li, L. C.; Liao, D. Z. *Dalton Trans.* **2009**, 8489. (h) Wang, X.-L.; Li, L.-C.; Liao, D.-Z. *Inorg. Chem.* **2010**, *49*, 4735. (i) Coronado, E.; Giménez-Saiz, C.; Recuenco, A.; Tarazon, A.; Romero, F. M.; Camon, A.; Luis, F. *Inorg. Chem.* **2011**, *50*, 7370.

(7) (a) Bogani, L.; Sangregorio, C.; Sessoli, R.; Gatteschi, D. *Angew. Chem., Int. Ed.* **2005**, *44*, 5817. (b) Bernot, K.; Bogani, L.; Caneschi, A.; Gatteschi, D.; Sessoli, R. *J. Am. Chem. Soc.* **2006**, *128*, 7947. (c) Bernot, K.; Bogani, L.; Sessoli, R.; Gatteschi, D. *Inorg. Chim. Acta* **2007**, *360*, 3807. (d) Liu, R.; Ma, Y.; Yang, P.; Song, X.; Xu, G.; Tang, J.; Li, L.; Liao, D.; Yan, S. *Dalton Trans.* **2010**, *39*, 3321. (e) Liu, R.; Li, L.; Wang, X.; Yang, P.; Wang, C.; Liao, D.; Sutter, J.-P. *Chem. Commun.* **2010**, *46*, 2568. (f) Poneti, G.; Bernot, K.; Bogani, L.; Caneschi, A.; Sessoli, R.; Wernsdorfer, W.; Gatteschi, D. *Chem. Commun.* **2007**, 1807. (g) Bernot, K.; Pointillart, F.; Rosa, P.; Etienne, M.; Sessoli, R.; Gatteschi, D. *Chem. Commun.* **2010**, 6458. (h) Mei, X.-L.; Liu, R.-N.; Wang, C.; Yang, P.-P.; Li, L.-C.; Liao, D.-Z. *Dalton Trans.* **2012**, *41*, 2904.

(8) Milios, C. J.; Vinslava, A.; Wernsdorfer, W.; Moggach, S.; Parsons, S.; Perlepes, S. P.; Christou, G.; Brechin, E. K. *J. Am. Chem. Soc.* **2007**, *129*, 2754.

(9) Miyasaka, H.; Clérac, R.; Mizushima, K.; Suguira, K.; Yamashita, M.; Wernsdorfer, W.; Coulon, C. *Inorg. Chem.* **2003**, *42*, 8203.

(10) Pointillart, F.; Bernot, K.; Sessoli, R.; Gatteschi, D. *Chem.—Eur. J.* **2007**, *13*, 1602.

(11) Rancurrel, C.; Sutter, J.-P.; Kahn, O.; Guionneau, P.; Bravic, G.; Chasseau, D. *New J. Chem.* **1997**, *21*, 275.

(12) Richardson, M. F.; Wagner, W. F.; Sands, D. E. *J. Inorg. Nucl. Chem.* **1968**, *30*, 1275.

(13) (a) Rancurel, C.; Heise, H.; Kohler, F.-H.; Schatzschneider, U.; Rentschler, E.; Vidal-Gancedo, J.; Veciana, J.; Sutter, J.-P. *J. Phys. Chem. A* **2004**, *108*, 5903. (b) Rancurrel, C.; Sutter, J.-P.; Le Hoerff, T.; Ouahab, L.; Kahn, O. *New J. Chem.* **1998**, *22*, 1333. (c) Leznoff, D. B.; Rancurrel, C.; Sutter, J.-P.; Golhen, S.; Ouahab, L.; Rettig, S. J.; Kahn, O. *Mol. Cryst. Liq. Cryst.* **1999**, *334*, 425.

(14) (a) *CrysAlis CDD*; *CrysAlis RED*, version p 171.29.2; Oxford Diffraction: Oxfordshire, Great Britain, 2000. (b) Sheldrick, G. M. *SHELXL-97*; University of Göttingen: Göttingen, Germany, 1997.

(15) Midollini, S.; Orlandini, A.; Rosa, P.; Sorace, L. *Inorg. Chem.* **2005**, *44*, 2060.

(16) Rancurel, C.; Leznoff, D. B.; Sutter, J.-P.; Golhen, S.; Ouahab, L.; Kliava, J.; Kahn, O. *Inorg. Chem.* **1999**, *38*, 4753.

(17) (a) Muetterties, E. L.; Guggenberg, L. J. *J. Am. Chem. Soc.* **1974**, *96*, 1748. (b) Drew, M. G. B. *Coord. Chem. Rev.* **1977**, *24*, 179.

(18) Okada, K.; Nagao, O.; Mori, H.; Kozaki, M.; Shiomi, D.; Sato, K.; Takui, T.; Kitagawa, Y.; Yamaguchi, K. *Inorg. Chem.* **2003**, *42*, 3221.

(19) Benelli, C.; Gatteschi, D. *Chem. Rev.* **2002**, *102*, 2369.
(20) Benelli, C.; Caneschi, A.; Gatteschi, D.; Pardi, L. *Inorg. Chem.* **1992**, *31*, 741.
(21) (a) Benelli, C.; Caneschi, A.; Gatteschi, D.; Laugier, J.; Rey, P. *Angew. Chem., Int. Ed. Engl.* **1987**, *26*, 913. (b) Benelli, C.; Caneschi, A.; Gatteschi, D.; Pardi, L.; Rey, P.; Shum, D. P.; Carlin, R. L. *Inorg. Chem.* **1989**, *28*, 272. (c) Benelli, C.; Caneschi, A.; Gatteschi, D.; Guillou, O.; Pardi, L.; Rey, P. *Inorg. Chim. Acta* **1989**, *160*, 1. (d) Benelli, C.; Caneschi, A.; Fabretti, A. C.; Gatteschi, D.; Pardi, L. *Inorg. Chem.* **1990**, *29*, 4153. (e) Benelli, C.; Caneschi, A.; Gatteschi, D.; Pardi, L.; Rey, P. *Inorg. Chem.* **1990**, *29*, 4223.
(22) Kahn, O. *Molecular Magnetism*; VCH: New York, 1993.
(23) Benelli, C.; Caneschi, A.; Gatteschi, D.; pardi, L.; Rey, P. *Inorg. Chem.* **1989**, *28*, 3230.
(24) (a) Sutter, J.-P.; Kahn, M. L. *Magnetism: Molecules to Materials*; Wiley-VCH: Weinheim, Germany, 2005. (b) Rinehart, J. D.; Long, J. R. *Chem. Sci* **2011**, *2*, 2078.
(25) Caneschi, A.; Ferraro, F.; Gatteschi, D.; Rey, P.; Sessoli, R. *Inorg. Chem.* **1990**, *29*, 1756. Caneschi, A.; Ferraro, F.; Gatteschi, D.; Rey, P.; Sessoli, R. *Inorg. Chem.* **1990**, *29*, 4217. Fettouhi, M.; Khaled, M.; Waheed, A.; Golhen, S.; Ouahab, L.; Sutter, J.-P.; Kahn, O. *Inorg. Chem.* **1993**, *38*, 3967.
(26) (a) Pasatoiu, T. D.; Etienne, M.; Madalan, A. M.; Andruh, M.; Sessoli, R. *Dalton Trans.* **2010**, *39*, 4802. (b) Ishikawa, N.; Sugita, M.; Wernsdorfer, W. *Angew. Chem., Int. Ed.* **2005**, *44*, 2931.
(27) (a) Gatteschi, D.; Sessoli, R. *Angew. Chem., Int. Ed.* **2003**, *42*, 268. (b) Jiang, S.-D.; Wang, B.-W.; Sun, H.-L.; Wang, Z.-M.; Gao, S. *J. Am. Chem. Soc.* **2011**, *133*, 4730. (c) Rebilly, J. N.; Catala, L.; Guillot, R.; Wernsdorfer, W.; Mallah, T. *Inorg. Chem.* **2005**, *44*, 8194. (d) Rebilly, J. N.; Catala, L.; Rivière, E.; Guillot, R.; Wernsdorfer, W.; Mallah, T. *Chem. Commun.* **2006**, 735. (e) Martinez-Lillo, J.; Armentano, D.; De Munno, G.; Wernsdorfer, W.; Julve, M.; Lloret, F.; Faus, J. *J. Am. Chem. Soc.* **2006**, *128*, 14218. (f) Martinez-Lillo, J.; Armentano, D.; De Munno, G.; Wernsdorfer, W.; Clemente-Juan, J. M.; Krystek, J.; Lloret, F.; Julve, M.; Faus, J. *Inorg. Chem.* **2009**, *48*, 3027. (g) Ferbinteanu, M.; Kajiwara, T.; Choi, K.-Y.; Nojiri, H.; Nakamoto, A.; Kojima, N.; Cimpoesu, F.; Fujimura, Y.; Takaishi, S.; Yamashita, M. *J. Am. Chem. Soc.* **2006**, *128*, 9008.
(28) Costes, J.-P.; Auchel, M.; Dahan, F.; Peyrou, V.; Shova, S.; Wernsdorfer, W. *Inorg. Chem.* **2006**, *45*, 1924.
(29) Costes, J.-P.; Clemente-Juan, J. M.; Dahan, F.; Milon, J. *Inorg. Chem.* **2004**, *43*, 8200.
(30) Cole, K. S.; Cole, R. H. *J. Chem. Phys.* **1941**, *9*, 341.
(31) (a) Dekker, C.; Arts, A. F. M.; Wijn, H. W.; van Duyneveldt, A. J.; Mydosh, J. A. *Phys. Rev. B* **1989**, *40*, 11243. (b) Aubin, S. M. J.; Sun, Z.; Pardi, L.; Krzystek, J.; Folting, K.; Brunel, L.-C.; Rheingold, A. L.; Christou, G.; Hendrickson, D. *Inorg. Chem.* **1999**, *38*, 5329.
(32) Gatteschi, D.; Sessoli, S.; Villain, J. *Molecular Nanomagnets*; Oxford University Press: Oxford, U. K., 2006.
(33) Mydosh, J. A. *Spin Glasses: An Experimental Introduction*; Taylor & Francis: London, 1993.
(34) Coulon, C.; Miyasaka, H.; Clérac, R. *Single-Molecule Magnets and Related Phenomena*; Winpenny, R., Ed.; Springer-Verlag Berlin: Berlin, 2006.
(35) (a) Ferbinteanu, M.; Miyasaka, H.; Wernsdorfer, W.; Nakata, K.; Sugiura, K.; Yamashita, M.; Coulon, C.; Clérac, R. *J. Am. Chem. Soc.* **2005**, *127*, 3090. (b) Lecren, L.; Roubeau, O.; Coulon, C.; Li, Y.-G.; Le Goff, X. F.; Wernsdorfer, W.; Miyasaka, H.; Clérac, R. *J. Am. Chem. Soc.* **2005**, *127*, 17353.